Thermal stability, electrical and magnetic properties of icosahedral $Al_{70}Pd_{20}Fe_{10-x}Mn_x$ alloys

1994 J. Phys.: Condens. Matter 6 10747

(http://iopscience.iop.org/0953-8984/6/49/016)

J. Phys.: Condens. Matter 6 (1994) 10747–10758. Printed in the UK

Thermal stability, electrical and magnetic properties of icosahedral $Al_{70}Pd_{20}Fe_{10-x}Mn_x$ alloys

C R Wang†, S T Lin† and Y C Chen‡

† Department of Physics, National Cheng Kung University, Tainan, Taiwan, Republic of China

‡ Materials Research Laboratories, Industrial Technology Research Institute, Hsinchu, Taiwan, Republic of China

Received 2 February 1994, in final form 28 July 1994

Abstract. Substitution of Fe for Mn in i-$Al_{70}Pd_{20}Fe_{10-x}Mn_x$ was found to decrease the thermal stability of the alloys. All Mn-containing alloys exhibit paramagnetic behaviour and have an effective magnetic moment per Mn atom in the range (1.39–1.86)μ_B. Measurements of the temperature dependence of the resistivity of this series of alloys reveal that the $Al_{70}Pd_{20}Fe_{10}$ alloy has the highest resistivities, 5600 $\mu\Omega$ cm and 5800 $\mu\Omega$ cm, at room temperature and at 5 K, respectively, and the Kondo effect is observed in Mn-containing alloys.

It was found that the resistivity behaviour can be varied quite significantly by varying the quenching rate.

1. Introduction

Since the discovery of an icosahedral phase (i-phase) with fivefold symmetry in rapidly quenched alloys of Al–Mn [1], the physical properties of the new materials have interested many physicists. In early studies of quasi-crystals, the Al–TM (TM ≡ transition metals) alloys were the main object. These alloys are simple icosahedral (SI) phases (P-type). They are usually unstable and hard to prepare as single i-phases [2]. In addition, these alloys contain many defects, chiefly owing to the distortion of the structure, and these structural imperfections could cause some uncertain effects on physical properties. The series of Al-based sp electron i-phase-like Al–Mg–(Ag, Cu, Zn) and (Al, Ga)–Mg–Zn alloys also have these disadvantages. The Al–Li–Cu–Mg [3] system was the first thermally stable i-phase discovered. Despite their good thermal stabilities, these alloys are still structurally disordered, as judged from the broadening in the x-ray peak width.

The discovery of thermally stable quasi-crystals Al–Cu–TM (TM ≡ V, Cr, Mn, Fe, Ru or Os) with a face-centred icosahedral (FCI) structure was first reported by Tsai *et al* [4]. The FCI structure (F-type) is distinguished from the SI phase (P type) by the existence of superlattice peaks in the x-ray diffraction pattern. The new electron diffraction spots would be introduced by the FCI structure along threefold and fivefold directions at multiples $\tau(=(\sqrt{5}+1)/2)$, instead of a sequence increasing by a scaling factor of τ^3 [5]. We can describe the FCI quasi-crystal as having a perfect long-range superlattice of a SI quasi-crystal. However, mainly owing to phason strains induced by quenching process, the structure of the Al–Cu–Fe quasi-crystals is also quite distorted. Perfect samples can be prepared only by annealing the samples at about 820 °C [6].

Recently Tsai *et al* [7] found a new series of icosahedral Al–Pd–Mn alloys. They found that, when the number of Pd atoms is increased, the structure of alloys can be transformed

0953-8984/94/4910747+12$19.50

from the SI to the FCI structure. Also, the as-quenched i-$Al_{70}Pd_{20}Mn_{10}$ was found to have a very small x-ray peak broadening [8], suggesting that there are nearly no frozen phason strains in the samples. This was attributed to chemical ordering caused by strong bonding between Pd and Al or Mn atoms [8]. Consequently, these alloys provide physicists with a good opportunity for studying the intrinsically physical properties of quasi-crystals without the influence of phason strains. Studies of the structure, magnetic and electronic properties of i-(Al–Pd–Mn) alloys have been reported [9–11, 14, 20]. It was found that manganese possesses a giant magnetic moment but, as in other Mn-containing quasi-crystals, only some of the Mn have a magnetic moment, indicating that the magnetic properties of this series of icosahedral alloys are also inhomogeneous. Additionally, electrical resistance measurements on i-(Al–Pd–Mn) alloys [11] revealed that the temperature and magnetic field dependences are governed dominantly by the weak localization effect for the case of strong spin–orbit scattering, and for high Mn concentrations, a Kondo effect is observed.

In this work, we shall study the effects of Fe on the thermal stability, magnetic and electrical properties of i-$Al_{70}Pd_{20}Fe_{10-x}Mn_x$ alloys.

2. Experimental procedure

Alloys of the series $Al_{70}Pd_{20}Fe_{10-x}Mn_x$ with $x = 0$, 2, 4, 6, 8 and 10 were prepared by arc melting a mixture of high-purity (99.999%) Al, high-purity (99.9%) Pd, high-purity (99.99%) Mn and high-purity (99.99%) Fe in a purified argon atmosphere. These alloy ingots were melted by induction in a quartz tube. Then the melts were rapidly quenched by ejection upon a single copper wheel with a diameter of 14.5 cm through an orifice 0.3 mm in diameter with argon gas. The structure was examined with a transmission electron microscope and an x-ray powder diffractometer. The thermal stability of the samples was studied by means of differential thermal analysis (DTA) measurements. DTA measurements were performed, under an argon atmosphere, at a heating rate of 20 °C min^{-1} from 500 to 1100 °C. DC susceptibilities were measured with a SQUID susceptometer in the temperature range from 5 to 300 K under an applied magnetic field of 10 kG. The conventional four-point probe technique was used for electrical resistance measurements.

3. Results and discussion

In the present work, $Al_{70}Pd_{20}Fe_{10-x}Mn_x$ alloys with $x = 0$, 2, 4, 6, 8 and 10 have been examined using transmission electron microscopy. Typical electron diffraction patterns of a quasi-crystal which show fivefold, threefold and twofold symmetrical diffraction spots are displayed in figures 1(*a*), (*b*) and (*c*), respectively. The x-ray powder diffraction patterns are shown in figure 2. The diffraction peaks can be indexed by six independent Miller indices following the scheme proposed by Elser. For samples with $x = 0$ and $x = 10$, the diffraction peaks were the same as those reported by Yokoyama *et al* [12]. A possible impurity phase indicated by an arrow was observed in the x-ray diffraction pattern of the sample with $x = 0$. The appearance of the superlattice peak of $\frac{1}{2}(311111)$ indicates that the structure of alloys is FCI (F type).

According to Elser's definition [13], we can calculate the quasi-lattice constant a, which is the length of the edge of the rhombohedral cells that make up the three-dimensional Penrose tiling, from the position of peak (211111). The results are shown in figure 1(*d*). The quasi-lattice constant a increases linearly as the concentration of manganese is increased.

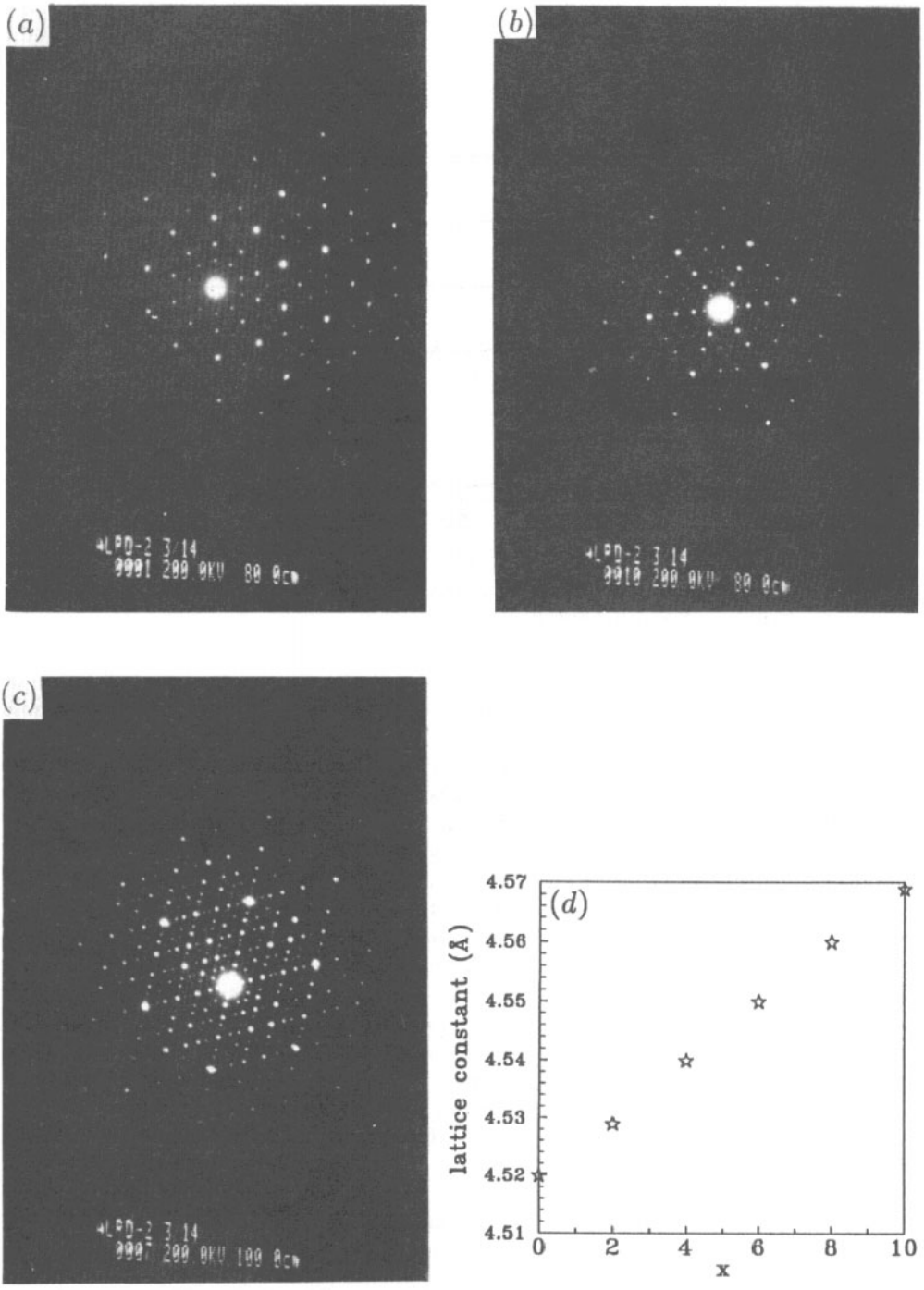

Figure 1. (*a*) Fivefold, (*b*) threefold and (*c*), twofold electron diffraction patterns of $Al_{70}Pd_{20}Fe_6Mn_4$. (*d*) Quasi-lattice constant as a function of Mn content for $Al_{70}Pd_{20}Fe_{10-x}Mn_x$.

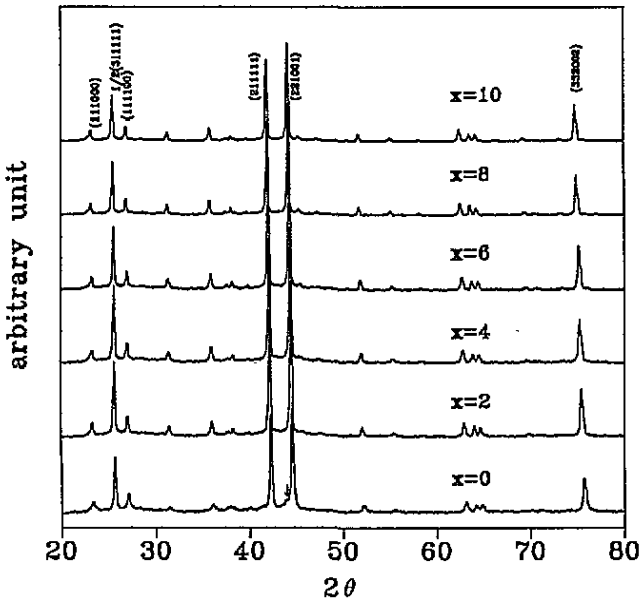

Figure 2. Room-temperature x-ray diffraction patterns for $Al_{70}Pd_{20}Fe_{10-x}Mn_x$ quasi-crystals with $x = 0, 2, 4, 6, 8$ and 10.

This can be interpreted by the fact that the atomic radius of manganese is larger than that of iron; the systematic increase in a may indicate that iron has indeed substituted for manganese in the quasi-crystalline structure of $Al_{70}Pd_{20}Mn_{10}$.

Figure 3 displays the DTA traces of $Al_{70}Pd_{20}Fe_{10-x}Mn_x$ quasi-crystals in the temperature range 700–1100 °C. No obvious exothermic peak indicating the transformation from i-phase to crystalline phase was found. Two clearly endothermic peaks are observed in the alloys with less than 8% Mn. T_m (indicated in the figure) is defined as the onset melting point. The temperatures at which two endothermic peaks appear are denoted by T_1 and T_2. The values of T_m, T_1 and T_2 are listed in table 1. It was seen that both T_m and T_1 decreased markedly as the Mn concentration was increased. Although no sample exhibits exothermic or endothermic peaks before the melting, we still cannot conclude that all the samples are in a thermodynamically stable phase. When $Al_{70}Pd_{20}Fe_{10-x}Mn_x$ quasi-crystals are annealed at an appropriate temperature lower than the melting points, we find an impurity phase appearing in the x-ray diffraction patterns of the alloys with less than 8% Mn. Figure 4 clearly shows that, after an anneal at 820 °C for 24 h, the i-$Al_{70}Pd_{20}Fe_4Mn_6$ already consisted of impurity phases, while the i-$Al_{70}Pd_{20}Fe_2Mn_8$ still retained its icosahedral structure. This indicates that the i-phases with more than 3% Fe atoms are not really thermodynamically stable.

Figure 5 shows the magnetization M versus applied field H at 5 K for $Al_{70}Pd_{20}Fe_{10-x}Mn_x$ (with $x = 0, 2, 4, 6, 8$ and 10) quasi-crystals. It can be seen that M is almost independent of H for the sample without Mn, i.e. $x = 0$, but it increases more rapidly with increasing applied field as the concentration of Mn is increased. This suggests that the magnetic properties of this series of alloys like other Al–Mn quasi-crystals mainly come from the contribution of the Mn component. In addition, we see that the magnetization does not saturate for applied fields up to 50 kG. The susceptibility and the inverse of the susceptibility plotted against temperature are shown in figures 6(a) and 6(b), respectively.

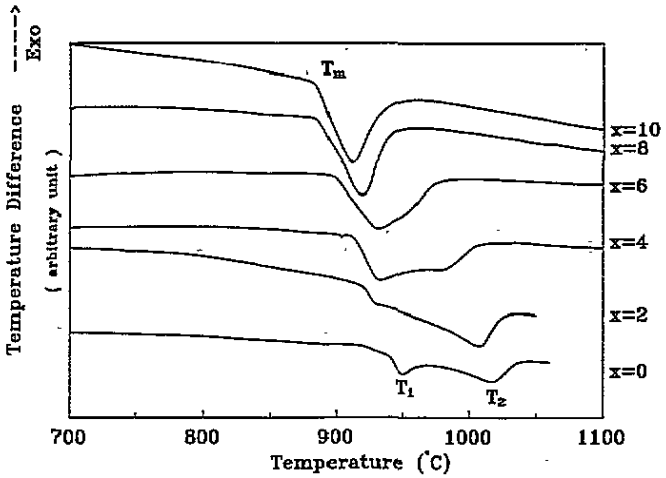

Figure 3. DTA traces of $Al_{70}Pd_{20}Fe_{10-x}Mn_x$ quasi-crystals with $x = 0$, 2, 4, 6, 8 and 10.

Table 1. Results of DTA for $Al_{70}Pd_{20}Fe_{10-x}Mn_x$: T_m, melting point; T_1, first peak temperature; T_2, second peak temperature.

x	T_m (°C)	T_1 (°C)	T_2 (°C)
10	884.0	911.9	
8	891.7	919.3	
6	898.9	931.7	
4	914.1	932.8	981.9
2	920.1	929.2	1007.6
0	936.9	950.3	1018.2

As seen in figure 6(*b*), all the results except for the sample with $x = 0$ can be fitted well by the formula $\chi = \chi_0 + C/(T - \Theta)$ where χ_0 is the temperature-independent susceptibility, C is the Curie constant and Θ is the paramagnetic Curie temperature. The effective magnetic moment p_{eff} per Mn atom can be calculated from the formula $p_{eff} = (3Ak_BC)^{1/2}/(N_A\alpha)^{1/2}$, where k_B, A, N_A, α are the Boltzmann constant, the average atomic weight of the alloys, Avogadro's number and the concentration of Mn atoms, respectively. The determined parameters χ_0, C, p_{eff} and Θ are listed in table 2. The values of p_{eff} were calculated by assuming that only Mn atoms carry a magnetic moment. The negative Θ is common for the vast majority of paramagnetic quasi-crystals; this indicates a predominantly antiferromagnetic exchange interaction between magnetic ions. The values of χ_0 for $Al_{70}Pd_{20}Fe_{10-x}Mn_x$ with $x = 4$–10 are positive, while for $x = 2$ its value of $\chi_0 \simeq -3.63 \times 10^{-7}$ emu g^{-1} G^{-1} is negative, indicating that there is the diamagnetic contribution to the magnetic susceptibility. However, even for $x = 0$ the alloy still remains in a paramagnetic state. This is quite different from the finding that replacement of Mn by Pd in i-Al–Pd–Mn alloys can drastically change the value and sign of χ_0 and for lower Mn concentrations as in $Al_{70.5}Pd_{22}Mn_{7.5}$ it exhibits diamagnetic properties for $T > 30$ K [9]. The value of p_{eff} is in the range (1.39–1.86)μ_B. i-$Al_{70}Pd_{20}Fe_8Mn_2$ has the largest value of $p_{eff} = 1.86\mu_B$, but this value was determined by fitting the Curie–Weiss law to the data of $(\chi - \chi_0)^{-1}$ versus the temperature between 30 and 300 K. Below 30 K, we can see that the inverse susceptibility deviates

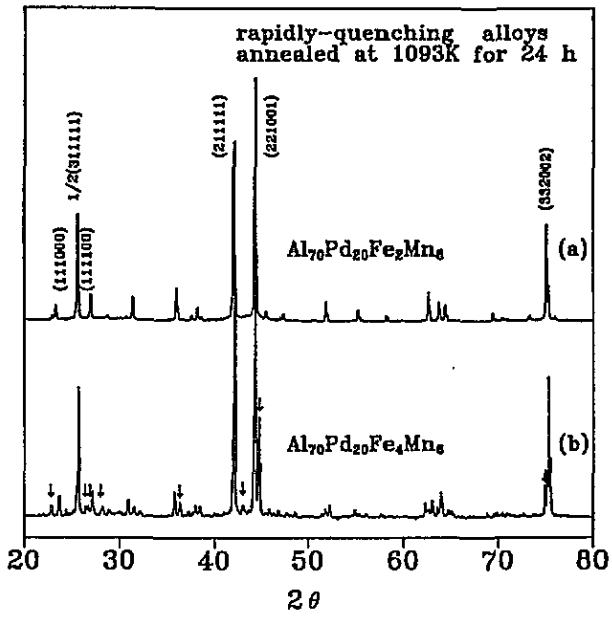

Figure 4. The x-ray diffraction patterns for the as-quenched $Al_{70}Pd_{20}Fe_2Mn_8$ (a) and $Al_{70}Pd_{20}Fe_4Mn_6$ (curve (b)) after annealing at 820 °C for 24 h.

downwards from the Curie–Weiss behaviour at high temperatures and the Curie–Weiss law can also be fitted to the data of $(\chi - \chi_0)^{-1}$ between 5 and 18 K with the parameters $p_{eff} = 1.37\mu_B$ and $\Theta \simeq -5.3$ K. Thus the Mn atom in $Al_{70}Pd_{20}Fe_8Mn_2$ carries two distinct values of p_{eff}. One value, $p_{eff} \simeq 1.86\mu_B$, is determined from the high-temperature fit and the other value, $p_{eff} \simeq 1.37\mu_B$ determined from the low-temperature fit is smaller. Two values of p_{eff} which differ much more were also observed in $Al_{70}Pd_{21}Mn_9$ and were attributed possibly to the formation of nearly compensated antiferromagnetic clusters [14].

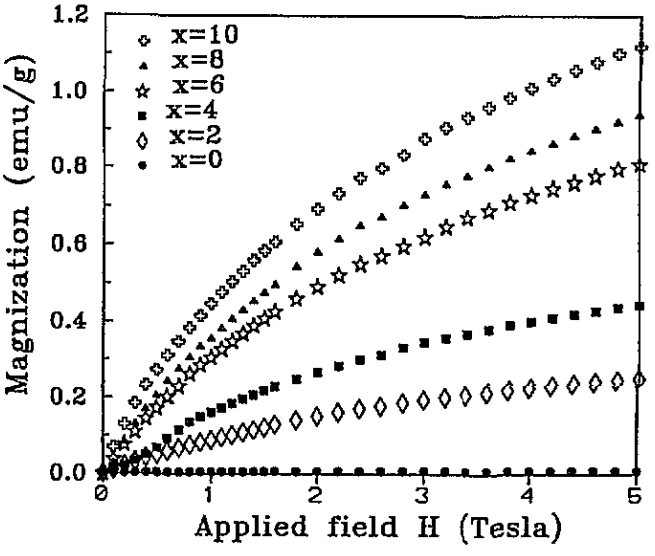

Figure 5. Magnetization versus applied field for $Al_{70}Pd_{20}Fe_{10-x}Mn_x$ ($x = 0, 2, 4, 6, 8$ and 10) at $T = 5$ K.

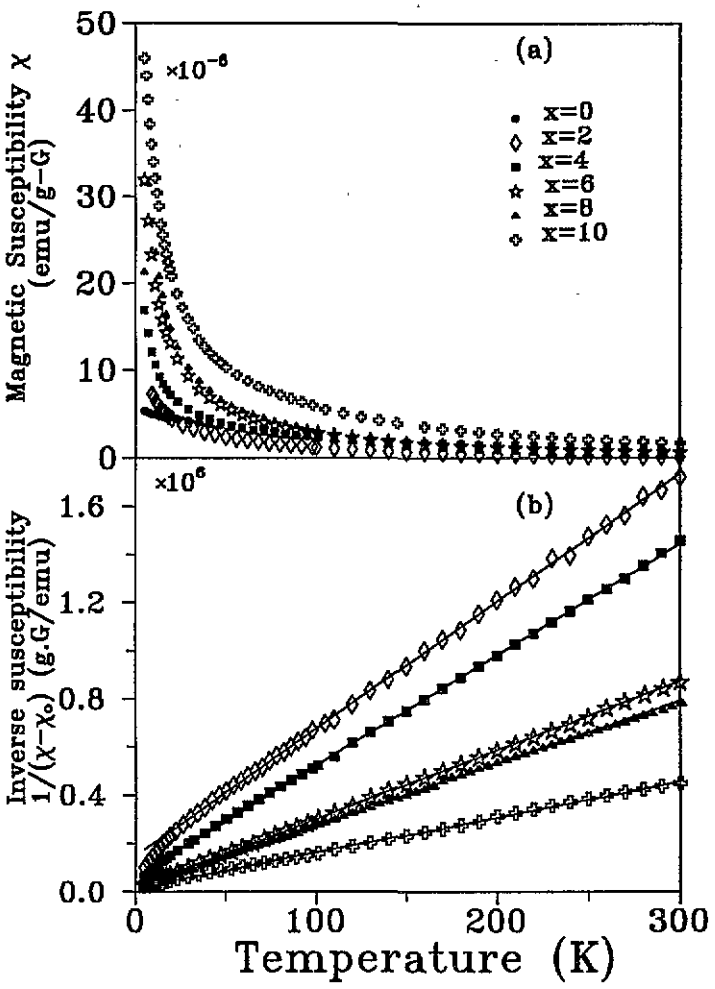

Figure 6. (*a*) Magnetic susceptibility χ versus temperature for $Al_{70}Pd_{20}Fe_{10-x}Mn_x$ with $x = 0$, 2, 4, 6, 8 and 10 under an applied field $H = 10^4$ G. (*b*) Inverse susceptibility $1/(\chi - \chi_0)$ versus temperature for $Al_{70}Pd_{20}Fe_{10-x}Mn_x$.

Table 2. The determined values of temperature-independent susceptibility χ_0, Curie constant C, the effective magnetic moment p_{eff}, the Curie temperature Θ as functions of x for the concentration α_m of magnetic Mn atoms, and the fraction $N^*/N(=\alpha_m/\alpha)$ of magnetic Mn for $Al_{70}Pd_{20}Fe_{10-x}Mn_x$.

x	$\chi_0(\times10^{-7})$ (emu g^{-1} G^{-1})	$C(\times10^{-4})$ (emu K g^{-1} G^{-1})	p_{eff} (μ_B)	α_m ($\times10^{-3}$)	N^*/N (%)	Θ (K)
10	1.36	6.85	1.59	4.9	4.9	−12.0
8	5.11	4.23	1.39	3.1	3.8	−3.1
6	5.72	3.51	1.46	2.5	4.2	−6.3
4	9.21	2.17	1.45	1.6	3.9	−13.8
2	−3.63	1.89	1.86	1.4	6.8	−28.0

As mentioned previously, not all Mn atoms in Al–Pd–Mn quasi-crystals are all magnetic,

but it is impossible to determine the effective magnetic moment and the number of magnetic atoms, simultaneously, from the Curie constant. Fukamichi *et al* [10] solved this problem by first determining the saturation magnetization M_s per Mn atom and the Curie constant C of $Al_{70}Pd_{20}Mn_{10}$ separately and then using the relation between M_s and C, i.e.

$$M_s\left(M_s\frac{N}{N^*}+g\mu_B\right)=\frac{3k_BC}{N}$$

to calculate the fraction N^*/N of magnetic Mn atoms, where N is the number of Mn atoms and N^* the number of magnetic Mn atoms and the g-value is taken to be 2. Assuming that a $1/H$ law holds for the high-field magnetization as it approaches saturation, they determined the M_s-value by scaling with the data on Cu–Mn crystalline dilute alloys and determined the effective magnetic moment p^*_{eff} per magnetic Mn atom and N^*/N to be $7.11\mu_B$ and 6.8% for $Al_{70}Pd_{20}Mn_{10}$. This indicates that Mn atoms carry a giant magnetic moment and the alloy can be regarded as a magnetically dilute alloy. Since our magnetization measured up to 5 T is still far from the saturation value, the value of M_s cannot be determined as Fukamichi *et al* did. Therefore, to determine N^*/N in our samples, we made the following assumptions:

(1) The magnetic moment of Fe is assumed to be negligible. This may be justified by the weak response of magnetization M to the applied magnetic field (see figure 5) and no Kondo effect observed in $Al_{70}Pd_{20}Fe_{10}$.

(2) Replacement of Mn by Fe does not change s^*, it varies only N^*.

Since the Curie constant C can be written

$$C=\frac{P^2_{eff}N_A\alpha}{3k_BA}=\frac{P^{*2}_{eff}N_A\alpha_m}{3k_BA}$$

where $p^2_{eff}=g^2s(s+1)$, $p^{*2}_{eff}=g^2s^*(s^*+1)$, s^* is the true value of the spin and α_m is the concentration of magnetic Mn atoms, we can calculate α_m as a function of Mn content in $Al_{70}Pd_{20}Fe_{10-x}Mn_x$ from the measured C by using the value of s^* (= 3.09) determined by Fukamichi *et al* [10]. The values of α_m and N^*/N determined for $Al_{70}Pd_{20}Fe_{10-x}Mn_x$ are listed in table 2. Our value of N^*/N (4.9%) for $Al_{70}Pd_{20}Mn_{10}$ is about 28% lower than the value (6.8%) determined by Fukachimi *et al*. This may be due to the differences in both the quenching conditions and the actual composition of the sample. The concentration α_m of magnetic Mn atoms is seen to decrease with increasing Fe content. This suggests that Fe substitutes for Mn in $Al_{70}Pd_{20}Mn_{10}$ possibly randomly and is contrary to what is observed in i-Al–(Mn–Fe)–Si where, at low Fe concentrations, Fe only substituties for Mn in non-magnetic sites [15], so that the concentration of magnetic Mn atoms is kept constant. The values of the fraction N^*/N of magnetic Mn atoms are more scattered; the average value is about 4.2(±0.4)%.

The normalized resistivity $\rho(T)/\rho(300\text{ K})$ for $Al_{70}Pd_{20}Fe_{10-x}Mn_x$ (x = 0, 2, 4, 6, 8 and 10) as a function of temperature is displayed in figure 7. All samples have high room-temperature resistivity (2200–5600 $\mu\Omega$ cm). A large negative temperature coefficient of resistivity was found for $Al_{70}Pd_{20}Fe_{10}$ and for $Al_{70}Pd_{20}Fe_{10-x}Mn_x$ (x = 2–10) in the range 120–300 K. For samples containing Mn, $\rho(T)$ exhibits a maximum between 40 and 120 K and a minimum for $T < 30$ K. Below the resistivity-minimum temperature, $\rho(T)$ is seen to increase logarithmically with decreasing temperature (see the inset of figure 7). Table 3 lists the resistivity-minimum temperature T_{min} and resistivity-maximum temperatures T_{max},

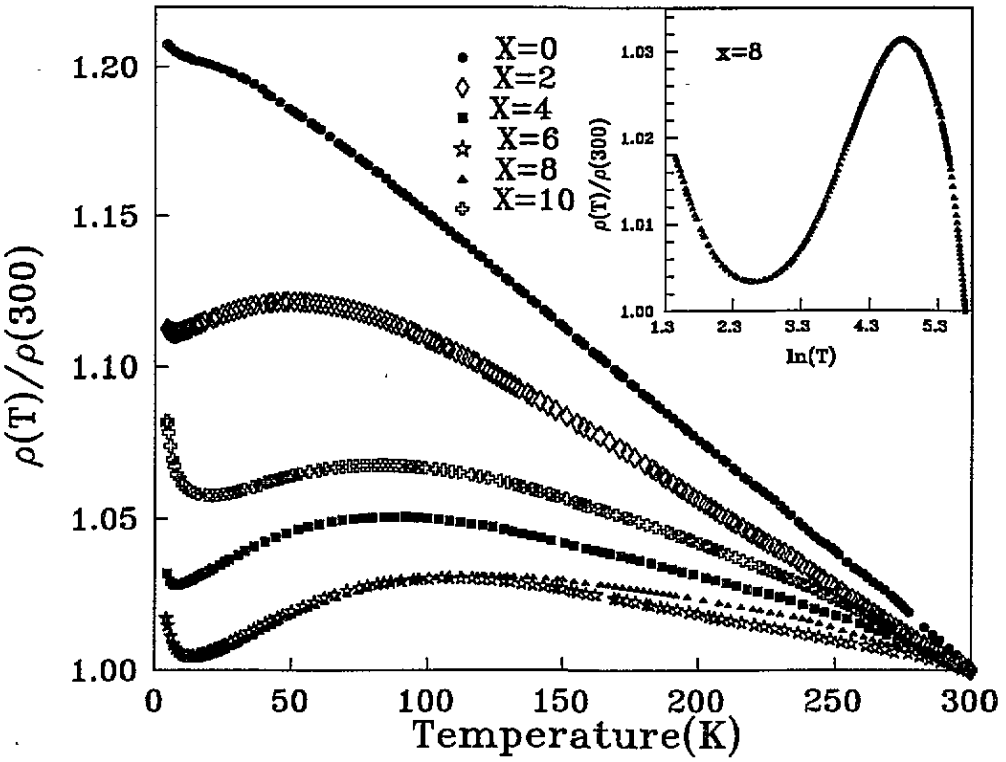

Figure 7. Temperature dependence of the normalized resistivity $\rho(T)/\rho(300\ \mathrm{K})$ for $Al_{70}Pd_{20}Fe_{10-x}Mn_x$ with $x = 0, 2, 4, 6, 8$ and 10. The inset shows the temperature dependence of the normalized resistivity against $\ln T$ for $Al_{70}Pd_{20}Fe_2Mn_8$.

Table 3. The measured values of the resistivity-minimum temperature T_{min} and the resistivity-maximum temperature T_{max}, the temperature coefficient of resistivity (TCR), $\rho^{-1}\,d\rho/dT$ at 300 K and the room-temperature resistivity $\rho(300\ \mathrm{K})$ for $Al_{70}Pd_{20}Fe_{10-x}Mn_x$.

x	T_{min} (K)	T_{max} (K)	$\rho^{-1}\,d\rho/dT$ at 300 K	$\rho(300\ \mathrm{K})$ ($\mu\Omega$ cm)
10	20	83	-5.0×10^{-4}	2800
8	14	107	-2.9×10^{-4}	3300
6	12	108	-2.3×10^{-4}	2200
4	9	89	-3.9×10^{-4}	2200
2	7	51	-5.5×10^{-4}	3000
0			-8.0×10^{-4}	5600

the temperature coefficient of resistivity (TCR) (equal to $d\rho/(\rho\,dT)$) at room temperature and the room-temperature resistivity $\rho(300\ \mathrm{K})$.

Conventionally, the $\ln T$ behaviour of resistivity at low temperatures can be contributed by two effects: one is the magnetic Kondo effect [16] caused by spin-flip scattering often found in crystals and amorphous alloys containing dilute magnetic impurity, and the other is the structural Kondo effect [17] due to the tunnelling effect of electrons between different local structures commonly observed in amorphous alloys. The former is influenced significantly by the change in concentration of magnetic atoms and applied magnetic field,

but the latter is not. The fact that T_{min} increases with increasing concentration of Mn in $Al_{70}Pd_{20}Fe_{10-x}Mn_x$ (see table 3) indicates that the increase in $\rho(T)$ at low temperatures originates from the magnetic Kondo effect. The same effect was also observed in quasi-crystal Al–Mn alloys [18]. If we consider that the resistivity has the phenomenological form $\rho(T)/\rho(300\ \mathrm{K}) = A - B\alpha_m \ln T + CT^n$ [19] near T_{min}, where A, B and C are constants and α_m is the concentration of magnetic impurities, then we shall have $T_{min} = (B\alpha_m/nC)^{1/n}$ and obtain the relation: $\ln T_{min} = (\ln \alpha_m)/n + \text{constant}$. From the plot of $\ln T_{min}$ versus $\ln \alpha_m$ (see figure 8), we obtained the value of $n \simeq 1.32 \pm 0.05$. Thus $T_{min} = (56\alpha_m)^{0.76}$.

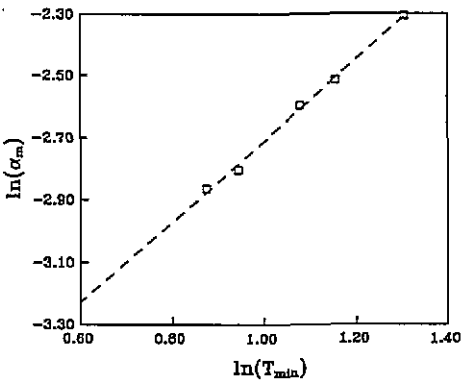

Figure 8. Logarithmic plot of the resistivity-minimum temperature T_{min} versus the concentration α_m of magnetic Mn, for $Al_{70}Pd_{20}Fe_{10-x}Mn_x$ with $x = 2$, 4, 6, 8 and 10.

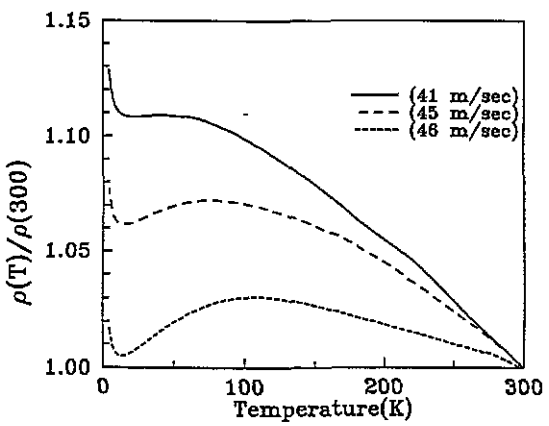

Figure 9. Temperature dependence of the normalized resistivity $\rho(T)/\rho(300\ \mathrm{K})$ for $Al_{70}Pd_{20}Fe_4Mn_6$ prepared with the different speeds of the copper wheel under a quenching process.

Quasi-crystals such as the series of Al–Cu–(Fe, Ru) and Al–Pd–Mn alloys with a resistivity of the order of 10^3–10^4 $\mu\Omega$ cm have a low density of states at the Fermi level and their temperature dependences of resistivity and magnetoresistivity can be fairly well

explained by considering the electron–electron interaction and weak localization effects [11, 20]. For the i-$Al_{70}Pd_{20}Fe_{10-x}Mn_x$ alloys studied, $Al_{70}Pd_{20}Fe_{10}$ has the highest room-temperature resistivity (5600 $\mu\Omega$ cm) and a negative TCR dominates over the temperature range 5–300 K. The other samples containing Mn have a room-temperature resistivity of about 2200–3300 $\mu\Omega$ cm. They all have a negative TCR at room temperature. However, as the temperature is decreased, all their resistivities reach a maximum. Below T_{max} their TCRs become positive. Akiyama *et al* [11] have shown that the positive TCR below T_{max} exhibited in the $\rho(T)$ curve of Al–Pd–Mn is governed dominantly by the weak localization effect including strong spin–orbit scattering, while weak spin–orbit scattering is more favourable in explaining the resistivity behaviour of $Al_{70}Pd_{20}Fe_{10}$, since it can only predict that $\rho(T)$ decreases linearly with increasing temperature.

Nevertheless, we note that the quenching process can affect the resistivity behaviour of these alloys greatly. Figure 9 shows the temperature dependence of the normalized resistivity for $Al_{70}Pd_{20}Fe_4Mn_6$ prepared with three different speeds of the copper wheel, which means different quenching rates by keeping other quenching conditions (such as the distance between the surface of the wheel and the tip of the quartz tube, the ejection pressure and the diameter of the orifice of the tube) fixed. The three samples prepared which were checked by x-ray diffraction are single i-phases but the diffraction patterns do not reveal any structural differences in these samples. The general features observed in figure 9 can be summarized as follows.

(1) A higher quenching rate decreases the magnitude of the TCR $d\rho/(\rho\, dT)$ at room temperature. In fact, it also decreases the resistivity of the sample, but this cannot be seen in figure 9 because only the normalized $\rho(T)/\rho(300\ K)$ is shown in the figure. Since a higher quenching rate usually induces more disorder in the quasi-periodic lattice, the above results indicate that, contrary to metallic samples, a quasi-crystal with more structural defects has a lower resistivity. Similar behaviour was also observed in i-(Al–Cu–(Fe, Ru)) [21] and i–Al–Pd–Mn [9] alloys.

(2) The resistivity-maximum temperature T_{max} moves towards low temperatures when the quenching rate is decreased.

(3) Reducing the quenching rate decreases the curvature of the $\rho(T)$ curve below T_{max}. For example, as the speed of the copper wheel equals 41 m s^{-1}, the resistivity maximum is barely seen.

(4) The resistivity-minimum temperature T_{min} is almost independent of quenching rate. This also provides evidence that the resistivity minimum appearing in the $\rho(T)$ curve of $Al_{70}Pd_{20}Fe_{10-x}Mn_x$ ($x = 2$–8) is indeed due to the magnetic scattering effect.

If the localization effect taking into account the strong spin–orbit scattering is mainly responsible for the resistivity behaviour of the series of Al–Pd–Fe–Mn alloys studied, then the fact that T_{max} and the curvature of the $\rho(T)$ curve can be varied greatly by varying the quenching rate implies that the weak localization effect can be enhanced or reduced, possibly by varying the quenching rate to modify the quasi-periodic structure microscopically.

Therefore, further studies on the connection of the weak localization effect with the quasi-periodic structure are needed to understand fully the resistivity behaviour of icosahedral alloys with a higher resistivity.

4. Summary

Some of the i-$Al_{70}Pd_{20}Fe_{10-x}Mn_x$ alloys with $x < 8$ can be transformed into a crystalline phase by annealing below their melting points, indicating that they are thermodynamically less stable than $Al_{70}Pd_{20}Mn_{10}$ alloy.

All Mn-containing alloys exhibit paramagnetic behaviour and the effective magnetic moments per Mn atom determined from their Curie constants are in the range (1.39–1.86)μ_B. The fraction of magnetic Mn atoms in this series of alloys is estimated to be about 4.2(±0.5)% (average value).

The i-$Al_{70}Pd_{20}Fe_{10-x}Mn_x$ alloys have high resistivities (2200–5600 $\mu\Omega$ cm) and their TCRs are all negative at room temperature. Both a resistivity minimum and a resistivity maximum are seen in the $\rho(T)$ curve of the Mn-containing alloys. The resistivity minimum is attributed to the Kondo effect.

It is found that the resistivity-maximum temperature and the curvature of the $\rho(T)$ can be varied by varying the quenching rate.

Acknowledgment

The authors are grateful to the National Science Council of Taiwan for partial support of this work.

References

[1] Shechtman D, Blech I, Gratias D and Cahn J W 1984 *Phys. Rev. Lett.* **53** 1951
[2] Dunlap R A and Dini K 1985 *Can. J. Phys.* **63** 1267
[3] Sainfort P, Dubost B and Dubus A 1985 *C. R. Acad. Sci., Paris* **10** 689
[4] Tsai A P, Inoue A and Masumoto T 1987 *Japan. J. Appl. Phys.* **27** L1587; 1988 *J. Mater. Sci. Lett.* **7** 322
[5] Mukhopadhyay N K, Ranganathan S and Chattopadhyay K 1987 *Phil. Mag. Lett.* **56** 121; 1989 *Phil. Mag. Lett.* **60** 207
[6] Waseda A, Edagawa K and Ino H 1990 *Phil. Mag. Lett.* **62** 183
[7] Tsai A P, Inoue A, Yokoyama Y and Masumoto T 1990 *Phil. Mag. Lett.* 619
[8] Tsai A P, Chen H S, Inoue A and Masumoto T 1991 *Phys. Rev.* **43** 8782
[9] Lanco P, Klein T, Berger C, Cyrot-Lackmann F, Fourcaudot G and Sulpice A 1992 *Europhys. Lett.* **18** 227
[10] Fukamichi K, Hattori Y, Nakane H and Goto T 1993 *Mater. Trans. Japan Inst. Met.* **34** 122
[11] Akiyama H, Hashimoto T, Shibuya T, Edagawa K and Takeuchi S 1993 *J. Phys. Soc. Japan* **62** 639
[12] Yokoyama Y, Tsai A P, Inoue A, Masumoto T and Chen H S 1991 *Mater. Trans. Japan Inst. Met.* **32** 421
[13] Elser V 1985 *Phys. Rev.* B **32** 4892
[14] Chernikov M A, Bernasconi A, Beeli C, Schilling A and Ott H R 1993 *Phys. Rev.* B **48** 3058
[15] Eibschütz M, Lines M E, Chen H S, Waszczak J V, Espinosa G P and Copper A S 1990 *Phys. Rev.* B **41** 4606
[16] Kondo J 1964 *Prog. Theor. Phys.* **32** 37
[17] Cochrane R W, Harris R, Ström-Olson J O and Zuckermann M J 1975 *Phys. Rev. Lett.* **35** 676
[18] Kimura K, Hashimoto T and Takeuchi S 1986 *J. Phys. Soc. Japan* **55** 1810
Gozlan A, Berger C, Fourcaudot G, Omari R, Lasjaunias J C and Préjean J J 1991 *Phys. Rev.* B **44** 575
[19] Hasegawa R and Tsuei C C 1970 *Phys. Rev.* B **2** 1631
[20] Chernikov M A, Bernasconi A, Beeli C and Ott H R 1993 *Europhys Lett.* **21** 767
[21] Kimura K, Kishi K, Hashimoto T and Takeuchi S 1991 *Proc. China–Japan. Semin. on Quasicrystals* ed K H Kuo and T Ninomiya (Singapore: World Scientific) p 233